RSC Advances

PAPER

View Article Online
View Journal | View Issue

Cite this: *RSC Adv.*, 2017, **7**, 50396

Synthesis and photoluminescence of Mn^{4+} activated ternary-alkaline fluoride K_2NaGaF_6 red phosphor for warm-white LED application†

Shijie Qiu, Hengwei Wei, Mengmeng Wang, Shuai Zhang, Yang Zhou, Ling Xu, Xiaoming Wang * and Huan Jiao *

A novel ternary-alkaline red emitting fluoride phosphor $K_2NaGaF_6:Mn^{4+}$ was successfully synthesized through co-precipitation method. The crystal structure, morphology, electronic band structure and luminescence properties of $K_2NaGaF_6:Mn^{4+}$ phosphors were investigated in details by using Rietveld refinement of X-ray diffraction data, scanning electron microscopy (SEM), density functional theory (DFT) calculation and different reaction parameters. The K_2NaGaF_6 host has a cubic unit cell with the space group $Fm\bar{3}m$ and lattice parameters of a = 8.2577 (4) Å, Z = 4, V_{cell} = 563.08 (8) Å^3. Under blue light excitation, Mn^{4+} activated K_2NaGaF_6 exhibits a bright narrow-band red emission. The PL properties of the $K_2NaGaF_6:Mn^{4+}$ red phosphors were optimized with different Mn^{4+} concentrations and aging times. A warm-white LED device was fabricated using a blue LED chip combined with commercial yellow $YAG:Ce^{3+}$ phosphor and synthesized $K_2NaGaF_6:Mn^{4+}$ red phosphor. The color rendering index (CRI, R_a = 81.6) and corresponding color temperature (CCT = 3643 K) easily reached the commercial warm white light LED standards (R_a > 80 and CCT < 4000 K). All these results indicate that $K_2NaGaF_6:Mn^{4+}$ phosphor would be a suitable red phosphor candidate for warm-white LED applications.

Received 15th September 2017
Accepted 21st October 2017

DOI: 10.1039/c7ra10274g

rsc.li/rsc-advances

1. Introduction

White light-emitting diodes (W-LEDs) received extensive attention in recent years, because of their outstanding advantages such as high efficiency, energy-saving, long-term reliability and environment friendliness.[1,2] Currently, the mainstream products of W-LEDs in the market are mainly packaged with blue InGaN chips and yellow phosphor $Y_3Al_5O_{12}:Ce^{3+}$ (YAG). However, due to the lack of red-emitting components, the related W-LEDs present a high correlated colour temperature (CCT > 4000 K) and a low colour rendering index (CRI, R_a < 80),[3–5] which result a cold white light emission. Therefore, exploring suitable red phosphors for W-LEDs is an important strategy to improve the luminescence quality of W-LEDs.

Recently, Mn^{4+} doped fluoride phosphors have been widely investigated due to their simple synthesis strategy and excellent luminescence properties.[4,6,7] They have a strong broad absorption in the near UV and blue region which match well with the UV and blue LED chips and emit a series of narrow red emissions from 600 nm to 650 nm. Compared to other W-LEDs red phosphors, Mn^{4+} doped fluoride shows better chemical stability than sulfide phosphors, and simpler synthesis conditions and lower cost than nitride phosphors. Many series of fluoride phosphors such as $A_2MF_6:Mn^{4+}$ (A = Na, K, Rb, Cs, M = Si, Ge, Sn, Zr, Ti),[8–15] $BMF_6:Mn^{4+}$ (B = Mg, Ca, Ba, Zn, M = Si, Ge, Ti)[16,17] and $A_3MF_6:Mn^{4+}$ (A = Na, K, M = Al, Ga)[18–22] have been reported. All of these Mn^{4+} activated fluorides phosphors exhibit intense broadband excitation and sharp red emission, which can be efficiently excited by near-UV or blue light and emit red light urgently required in warm W-LEDs.

Tuning phosphors emission bands is an important approach to improve the luminescence performance of W-LEDs. A usual way is to replace neighbour cations, changing the activator ions structure environment and making the luminescence properties change continuously. This strategy has been applied in many fluorides systems, for example, cubic elpasolite phosphors $A_2BLF_6:Mn^{4+}$ (A: larger alkali ion (K), B: smaller alkali ion (Na, Li), L: trivalent cation (Al, Sc, Ga)),[23–28] Mn^{4+} ions occupy the positions of Al^{3+}, Sc^{3+}, or Ga^{3+}. Recently, Wang group reported two novel Mn^{4+}-doped fluoride phosphors $K_2LiAlF_6:Mn^{4+}$ and $K_2NaAlF_6:Mn^{4+}$.[24,29] These substitutions are mainly focused on the A site and B site. In order to improve the luminescent properties of fluoride phosphors, for example luminous intensity, thermal quenching effect, quantum efficiency and so on, more attempts could be tried on L site or the 3 cations combinations. With diverse cation radius, different structure and luminescent properties can be expected.

Key Laboratory of Macromolecular Science of Shaanxi Province, School of Chemistry & Chemical Engineering, Shaanxi Normal University, Xi'an 710062, Shaanxi Province, P. R. China. E-mail: xmwang@snnu.edu.cn; jiaohuan@snnu.edu.cn

† Electronic supplementary information (ESI) available. See DOI: 10.1039/c7ra10274g

In this paper, we successfully synthesized a series of ternary-alkaline gallate fluoride red $K_2NaGaF_6:Mn^{4+}$ phosphors through co-precipitation method at room-temperature. This phosphor shows pale yellow in daylight and emits a narrow-band red light under blue light excitation. The crystal structure, morphology, composition, electronic band structure and luminescence properties were investigated in details. In addition, the reaction parameters such as Mn^{4+} doping concentration and aging time have been investigated to optimize the photoluminescence properties. Finally, we fabricated a warm W-LED using a blue LED chip combined with a yellow YAG:Ce^{3+} phosphor and a $K_2NaGaF_6:Mn^{4+}$ red phosphor, and the luminescence properties of this warm W-LED was obtained.

2. Experimental

2.1 Raw materials

The ternary-alkaline phosphors were synthesized from the raw chemicals KF (99.5%), NaF (99.99%), Ga_2O_3 (99.99%), acetone (A.R.) and HF (49%). Main chemicals were purchased from Aladdin Chemistry, China. All of these starting reagents were used directly without any further purification.

2.2 Synthesis method

Compounds of $K_2NaGaF_6:Mn^{4+}$ were prepared through a co-precipitation method according to ref. 31. In a typical procedure of preparing $K_2NaGaF_6:Mn^{4+}$ (see Fig. 1), 0.4686 g of Ga_2O_3 and different amount of K_2MnF_6 were dissolved in 15 mL HF solution under stirring. Then, 0.9682 g KF and 0.3449 g NaF were added into the solution. The mixed solution was stirred for 30 min. After putting the plastic beaker into ice-water bath for several hours, washed with acetone and dried at 70 °C for 2 h. The pale yellow powder of $K_2NaGaF_6:Mn^{4+}$ red phosphors were obtained.

For optimization of the luminescence performance, different concentrations of Mn^{4+} doped K_2NaGaF_6 samples were synthesized using different mole ratios of Ga to Mn and the real doped concentrations has been measured, as shown in Table 1.

2.3 Characterization

The crystal structures of the synthesized powders were analysed by a Rigaku MiniFlex 600 X-ray powder diffractometer. Powder's XRD data were collected in continuous scanning mode in a 2θ range of 10–80°, with a step size of 0.02°, a tube voltage of 40 kV, and a tube current of 15 mA. Rietveld refinements on X-ray diffraction data were performed using the software TOPAS 4.2.

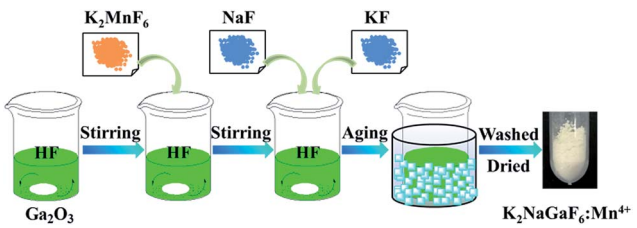

Fig. 1 Synthesis diagram of $K_2NaGaF_6:Mn^{4+}$ phosphors through co-precipitation method.

Table 1 Flame atomic absorption spectrophotometer (FAAS) results of $K_2NaGaF_6:Mn^{4+}$ phosphors prepared with different molar ratios of K_2NaGaF_6 to K_2MnF_6

Samples	Moar ratio of Ga to Mn	Dopant amount of Mn (mol%) in K_2NaGaF_6
S1	100 : 1.0	0.82
S2	100 : 1.5	1.33
S3	100 : 1.8	1.62
S4	100 : 2.0	1.76
S5	100 : 2.5	2.12
S6	100 : 3.0	2.67
S7	100 : 3.5	3.30

Density functional theory (DFT) calculation for K_2NaGaF_6 was performed with the Cambridge Serial Total Energy Package (CASTEP) code, in which a plane wave basis set was chosen for expansion of valence-electron wave functions at the local density approximation (LDA) level.[30] There were two steps of calculations to get the band structure of K_2NaGaF_6. The first step was to optimize its crystal structure using the Broyden–Fletcher–Goldfarb–Shannon (BFGS) method. The second step was to calculate the band structure and density of states (DOS). In this calculation, the energy cutoff was set as 450 eV. Criterion for the self-consistent field (SCF) was eigenenergy convergence within 1.0×10^{-7} eV per atom.

The morphology and EDX mapping of samples was investigated by scanning electron microscopy (SEM, Philips-FEI Quanta 200, America) with an attached energy-dispersive X-ray spectrometer (EDS, INCA-Oxford, High Wycombe, UK).

The Mn^{4+} content in samples was measured on a flame atomic absorption spectrophotometer (FAAS) TAS-990F (Beijing Purkinje General Instrument Co., Ltd., China). PL spectra were acquired with a Hitachi F-4600 fluorescence spectrophotometer with the excitation and emission slits set to 2.5 nm, and the xenon lamp was used as excitation source. The diffuse reflectance ultraviolet-visible spectra (DRS) were collected on a UV-vis-NIR spectrophotometer UV-lambda 950 (PerkinElmer General Instrument Co., Ltd., America). The luminescence quantum efficiencies of obtained samples were measured using a quantum efficiencies measurement system C9920-02G (Hamamatsu, Japan).

2.4 Fabrication of W-LEDs

For the purpose of exploring reliability under LED operating conditions, prototype W-LEDs were fabricated with commercial yellow phosphor YAG:Ce^{3+}, the synthesized red phosphor $K_2NaGaF_6:Mn^{4+}$ in this work, and blue InGaN chips. Luminescence properties of the obtained devices were measured at various drive current changed from 25 mA to 350 mA.

3. Results and discussion

3.1 Structure and spectroscopic analysis

Fig. 2 shows the crystal structure of K_2NaGaF_6 and XRD patterns of doped and non-doped K_2NaGaF_6. In Fig. 2(a), Ga^{3+} and Na^+

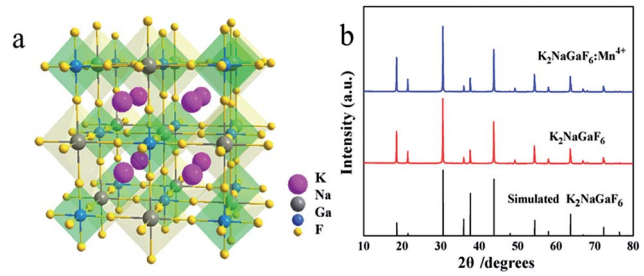

Fig. 2 (a) Structure diagram and (b) XRD patterns of K_2NaGaF_6 and $K_2NaGaF_6:Mn^{4+}$ (1.76 mol% Mn^{4+}).

ions are surrounded by six F^- ions to form $[GaF_6]$ and $[NaF_6]$ octahedrons ionic groups, respectively. K^+ ion locates at the centre of four octahedrons forming a $[KF_{12}]$ decahedral cage. The $[GaF_6]$ and $[NaF_6]$ octahedrons are linked through vertex-share F^- ions. The effective radius of Ga^{3+} ion and Mn^{4+} ion at a CN = 6 (CN = coordination number) are 0.62 Å and 0.53 Å, respectively.[20]

Fig. 2(b) shows XRD patterns of K_2NaGaF_6, $K_2NaGaF_6:Mn^{4+}$ as well as the simulated card of K_2NaGaF_6. With 1.76 mol% Mn^{4+} doping in K_2NaGaF_6, no impurity peaks were observed, which indicated the doped phosphor has a pure phase as the non-doped samples. Using K_2NaAlF_6 as a structure model, the Rietveld refinements based on powder XRD data indicated that the prepared K_2NaGaF_6 has the cubic unit cell with the space group $Fm\bar{3}m$ and lattice parameters of a = 8.2577 (4) Å, Z = 4 and V_{cell} = 563.08 (8) Å^3 (simulated) (in Table 2). The observed and calculated XRD patterns for K_2NaGaF_6, as well as difference profile are illustrated in Fig. 3. The refinement on XRD data shows a good fitting of residual factors R_p = 6.57%, R_{wp} = 8.54%, R_{exp} = 6.17%, and the GOF = 1.38 (Table 2).

The photoluminescence excitation (PLE) and photoluminescence (PL) spectra of red phosphor $K_2NaGaF_6:Mn^{4+}$ (1.76 mol% Mn^{4+}) are shown in Fig. 4(a). There are two excitation bands in PLE spectra, centred at 355 nm and 466 nm when monitored at 630 nm. The broad excitation bands are attributed to the spin-allowed and parity-forbidden transitions $^4A_{2g} \rightarrow {}^4T_{1g}$ and $^4A_{2g} \rightarrow {}^4T_{2g}$ of Mn^{4+}.[7,31]

Table 2 Crystallographic data of K_2NaGaF_6 derived from Rietveld refinement of X-ray diffraction data

Formula	K_2NaGaF_6
Crystal system	Cubic
Space group	$Fm\bar{3}m$
Lattice parameter a (Å)	8.2577 (4)
V_{cell} (Å^3)	563.08 (8)
Z	4
Temp. (K)	293
Profile range (°)	$10 \leq 2\theta \leq 80$
Profile function	PVII
No. of data points	3501
R_p (%)	6.57
R_{wp} (%)	8.54
R_{exp} (%)	6.17
GOF	1.38

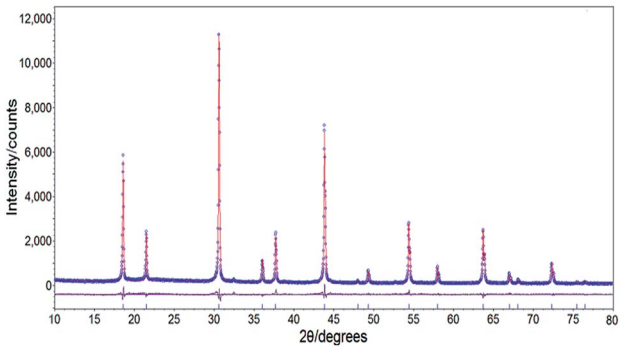

Fig. 3 Observed (blue dots) and calculated (red line) powder XRD patterns as well as difference profile (grey line) for Rietveld refinements of K_2NaGaF_6.

Under the excitation of 466 nm, the $K_2NaGaF_6:Mn^{4+}$ phosphors emit a series of narrow red emission lines located at 598 nm, 607 nm, 613 nm, 622 nm, 630 nm, 633 nm and 646 nm, which can be assigned to the transitions of anti-Stokes $v_3(t_{1u})$, $v_4(t_{1u})$, and $v_6(t_{2u})$, zero phonon line (ZPL), and Stokes $v_6(t_{2u})$, $v_4(t_{1u})$ and $v_3(t_{1u})$ vibronic modes respectively.[25,26] In Fig. 4(a), it is obvious that the ZPL of $K_2NaGaF_6:Mn^{4+}$ appears significantly stronger compared to $K_2SiF_6:Mn^{4+}$ or $K_2GeF_6:Mn^{4+}$ phosphor. Normally, the emission intensity of the ZPL is highly dependent on the local symmetry of Mn^{4+} surrounding. But, in this work it is attributed to the damage of symmetry of Mn^{4+} ion in K_2NaGaF_6 because of non-equivalent doping between Ga^{3+} and Mn^{4+}.[21] The phosphor colour is pale yellow and it emits an

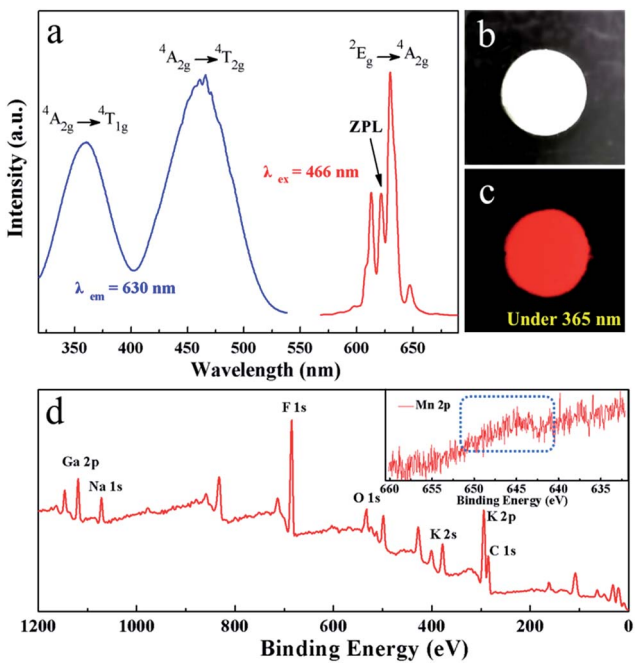

Fig. 4 (a) PLE and PL spectra (1.76 mol% Mn^{4+}), (b) image obtained under natural light (1.76 mol% Mn^{4+}), (c) image obtained under UV-light (1.76 mol% Mn^{4+}), and (d) XPS spectrum of $K_2NaGaF_6:Mn^{4+}$ (1.76 mol% Mn^{4+}). The inset is the magnification of Mn^{4+} part of the spectrum.

intense red light under blue light and UV light, as shown in Fig. 4(b) and (c).

The X-ray photoelectron spectroscopy (XPS) spectrum of K_2NaGaF_6:Mn^{4+} is shown in Fig. 4(d). The XPS spectrum depicts the potassium (K), sodium (Na), gallium (Ga), fluoride (F), and manganese (Mn) elements. There were little oxygen (O) and carbon (C) observed due to absorption of CO_2 or H_2O. Since the low concentration of Mn^{4+}, its peak is not so obvious. Hence, a magnification of Mn part of the spectrum is provided in the inset to show Mn element clearly.

3.2 Electronic band structure

The electronic structure of K_2NaGaF_6 was calculated with the CASTEP module of the Materials Studio package, and the results are shown in Fig. 5(a) and b. Obviously, the calculated indirect band gap of K_2NaGaF_6 is approximately 5.92 eV, that indicates K_2NaGaF_6 is a good luminescent host due to its wide band gap.[21] The top point on valence band and bottom point on conduction band both locate at the G point, which indicates that it is a direct band gap semiconductor. Fig. 5(b) shows the total and partial density of states (DOS) of K_2NaGaF_6. The conduction band is mainly composed by Ga/Na/K s and p orbitals, while the valence band is mainly composed by F 2p orbitals.

The UV-vis DRS of the representative non-doped K_2NaGaF_6 and Mn^{4+}-doped K_2NaGaF_6 are displayed in Fig. 6. The slightly decreasing reflectance of non-doped K_2NaGaF_6 (black solid line) from 200 to 320 nm is the same as other reported fluoride phosphor.[32–34]

The band gap is estimated according to eqn (1).

$$(\alpha h\nu)^n = A(h\nu - E_g) \quad (1)$$

where $h\nu$ is the incident photon energy; α is the absorption coefficient; A is a constant; $n = 1/2$ for an indirect transition or 2 for a direct transition.[35] The values of $(\alpha h\nu)^2$ are plotted as a function of the incident photon energy ($h\nu$) as illustrated in Fig. 6. From the linear extrapolation of $(\alpha h\nu)^2 = 0$, the E_g value was estimated to be about 5.98 eV, which is consistent with the value 5.92 eV determined from the DFT calculation.

In contrast with the non-doped host K_2NaGaF_6, the red phosphor K_2NaGaF_6:Mn^{4+} (1.76 mol%) sample has two intense

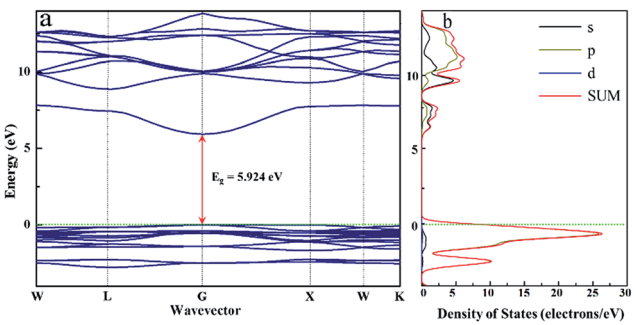

Fig. 5 (a) Calculated energy band structure, (b) the total and partial density of states of K_2NaGaF_6.

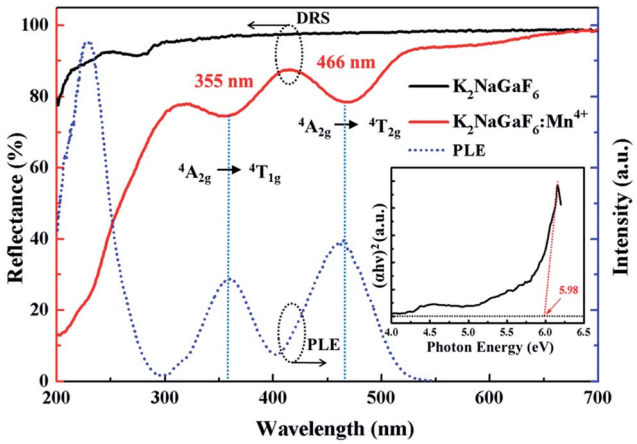

Fig. 6 DRS of the non-doped and Mn^{4+}-doped K_2NaGaF_6 and PLE of K_2NaGaF_6:Mn^{4+} (1.76 mol%). The inset shows the Tauc plot for the non-doped sample.

absorption bands at ~355 nm and ~466 nm, which are due to the spin-allowed transition of $^4A_{2g} \rightarrow {}^4T_{1g}$ and $^4A_{2g} \rightarrow {}^4T_{2g}$ of Mn^{4+}, respectively, as has also been clearly observed in the PLE spectrum. This result means that this phosphor can be effectively excited by blue InGaN chip, which shows great potential applications in W-LEDs.

3.3 Morphology and composition studies

The SEM and EDS analysis of K_2NaGaF_6:Mn^{4+} (1.76 mol%) show in Fig. 7. In Fig. 7(a), the synthesized K_2NaGaF_6:Mn^{4+} phosphor exhibited octahedral shaped crystals with particle size of 1.5–2.0 μm. The element contents were represented in the inset of Fig. 7(b). The atom ratios of K, Na, Ga, F are about 20.05%, 14.73%, 9.97%, 54.99% respectively, which is close to 2 : 1 : 1 : 6 ratio of K_2NaGaF_6.

3.4 Optimization of the reaction parameters

To optimize the photoluminescence properties of K_2NaGaF_6:Mn^{4+}, the effects of Mn^{4+} concentration and aging time were systematically investigated. As shown in Fig. S1(a) and (b),† the XRD patterns indicate that all the phosphors with a Mn^{4+} molar concentration range from 0.82% to 3.30% and different aging durations are all pure phase. Fig. 8(a) shows the emission spectra of K_2NaGaF_6:Mn^{4+} with different doping concentration. Under

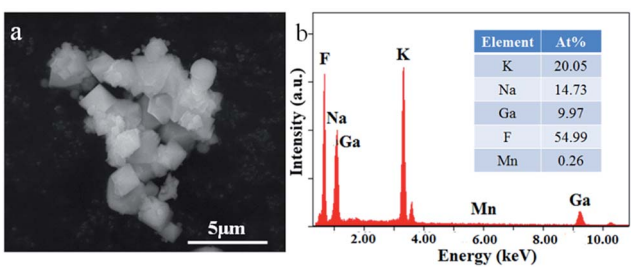

Fig. 7 (a) SEM and (b) quantitative elemental composition data of K_2NaGaF_6:Mn^{4+} (1.76 mol%).

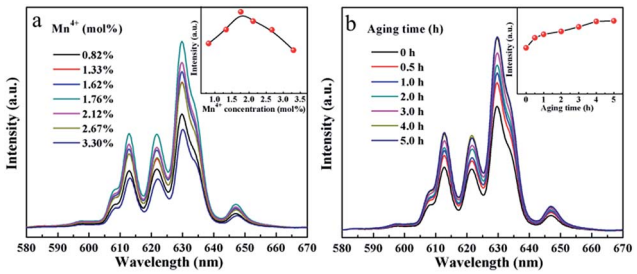

Fig. 8 PL spectra of K_2NaGaF_6:Mn^{4+} with different doping concentration (a) and aging time (b). The inset in (a) and (b) show the integrated emission intensity of K_2NaGaF_6:Mn^{4+}.

466 nm excitation, all the samples present a narrow red emission line centred at 630 nm. The relationship between integrated emission intensity and Mn^{4+}-doping concentration in K_2NaGaF_6:Mn^{4+} is shown in the inset of Fig. 8(a). In order to confirm the real concentration of Mn^{4+} in K_2NaGaF_6, FAAS was used to measure the Mn^{4+} content in these samples and the results are listed in Table 1. The real concentration of Mn^{4+} in these samples is increased with the consumption of K_2MnF_6, and the emission intensity reaches maximum at the value of 1.76 mol%. Beyond this concentration, the luminescence intensity starts to fall due to the concentration quenching of Mn^{4+} in the K_2NaGaF_6 crystal lattice. Under 466 nm light excitation, K_2NaGaF_6:Mn^{4+} (1.76 mol%) presents a quantum efficiency of 61.8%, better than K_2NaAlF_6:Mn^{4+} with 58.4%.[25]

It is well known that for phosphor particles, luminescence can be greatly affected by the crystallinity, surface defects, and doping concentration.[36–39] For fluoride phosphors synthesized by co-precipitation method, particles are formed in a very short time. Therefore, a period of time is needed to modify the atom position and decrease surface defects. Aging as an effective way to obtain high crystallinity and low surface defect crystals is an important approach to optimize PL properties of fluoride phosphor. The K_2NaGaF_6:Mn^{4+} phosphors in HF solution were aged in ice-water to improve the crystallinity of the particles. Fig. 8(b) shows the emission spectra of K_2NaGaF_6:Mn^{4+} red phosphors obtained after different aging times. The emission intensity of K_2NaGaF_6:Mn^{4+} reaches a maximum after 4 h reaction. Then the emission intensity invariant as the aging time increases further. From Fig. S2,† it is clearly that the crystallinity of K_2NaGaF_6:Mn^{4+} particles can be improved by increasing the aging time. With the prolonging of aging time, the particle size and shape of K_2NaGaF_6:Mn^{4+} changed gradually. The particle size increased from 0.7 μm to 2 μm and the morphology transformed from sphere to octahedron gradually. The crystal size of K_2NaGaF_6:Mn^{4+} particles with less than 1 h aging time are much small, and their octahedron sharps are also not clear. With more than 4 h aging time, particles show higher crystallinity and better luminescence properties. The K_2NaGaF_6:Mn^{4+} particles are composed of octahedral shaped crystals featured by clear edges and corners. It is believed that the optimal reaction conditions to obtain the red light K_2NaGaF_6:Mn^{4+} are about 4 h aging time with 1.76 mol% Mn^{4+} concentration.

Fig. 9 shows the concentration-dependent PL decay curves of Mn^{4+} in K_2NaGaF_6:Mn^{4+} red phosphors under 466 nm blue light excitation, the relationship between Mn^{4+} doping concentration and lifetime was shown in inset. The PL decay time was fitted based on a single-exponential function. As is shown in Fig. 9, the lifetimes of Mn^{4+} decay from 4.24 ms to 2.35 ms along with increasing of Mn^{4+} concentration from 0.82 mol% to 3.3 mol%. However, when the doping concentration of Mn^{4+} more than 2.1 mol%, the PL decay curves deviated the single-exponential decay trend. That can be explained by the serious non-radiative transition processes among the Mn^{4+} ions at a high Mn^{4+} concentration level.

3.5 LED application

In order to understand the features of K_2NaGaF_6:Mn^{4+} red phosphor and its application in the devices of warm W-LEDs, we fabricated a warm W-LED using a blue LED chip combined with the commercial yellow YAG:Ce^{3+} phosphor and the synthesized K_2NaGaF_6:Mn^{4+} (1.76 mol% Mn^{4+}) red phosphor. Fig. 10(a) shows the current-dependent LED performance of this combined device. The sharp red emission of K_2NaGaF_6:Mn^{4+} red phosphor at ~633 nm can be observed clearly in this electroluminescence (EL) spectra. The broad band centred at ~550 nm belongs to the emission of the YAG:Ce^{3+} yellow phosphor and the sharp peak at ~460 nm can be attributed to the emission of the InGaN chip.[12,19,31]

From Fig. 10(a), it is obviously that there is no remarkable change on band shapes and positions of emission peaks when the drive current increases from 20 to 350 mA. Moreover, the emission intensity increased with the increasing driven current. All these results indicate this warm W-LED has a good stability in CRI and CCT. Photographs of the W-LED device are shown in the inset image of Fig. 10(a). Owing to the red light in the emission spectrum, a noticeable warm light emission can be observed. The chromaticity coordinates value under different currents are labelled in Fig. S3† and CIE chromaticity diagram

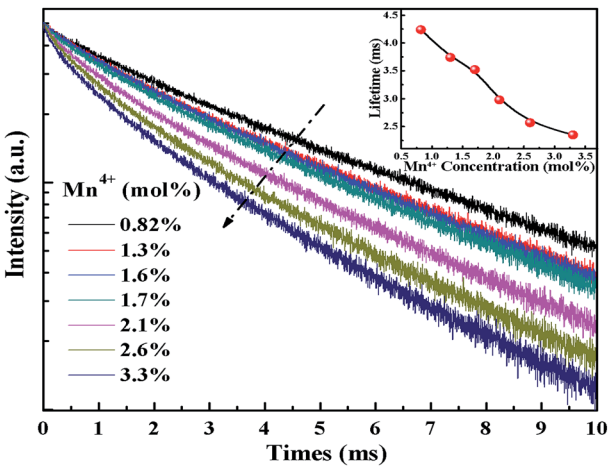

Fig. 9 Room temperature PL decay curves of K_2NaGaF_6 doped with different Mn^{4+} concentration. The inset shows the lifetimes of K_2NaGaF_6:Mn^{4+}.

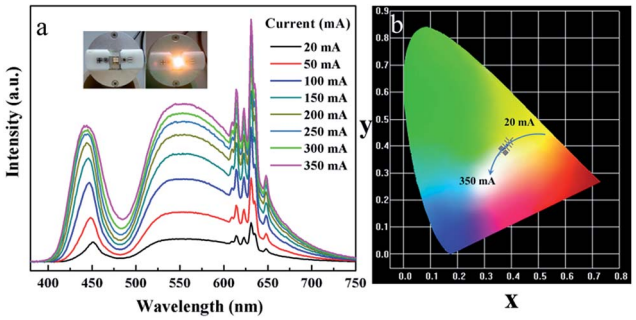

Fig. 10 (a) Electroluminescence spectra and (b) CIE chromaticity diagram of fabricated white LED under various drive currents.

Fig. 10(b). The R_a and CCT values of this W-LED are 81.6 and 3643 K respectively. Moreover, the colour tolerance adjustment (CTA) of this W-LED is 6.4 SDCM, which is very close to the commercial standard. All these results indicate the potential of $K_2NaGaF_6:Mn^{4+}$ phosphor as red component for W-LEDs application.

4. Conclusions

In summary, a highly efficient novel ternary-alkaline red emitting fluoride phosphor, $K_2NaGaF_6:Mn^{4+}$, has been successfully synthesized through co-precipitation method at room-temperature. The K_2NaGaF_6 host has a cubic unit cell with the space group $Fm\bar{3}m$ and lattice parameters of a = 8.2577 (4) Å, Z = 4, V_{cell} = 563.08 (8) Å^3. The band gap is approximately 5.92 eV calculated with the CASTEP, which very is close to the experimental result (5.98 eV). The morphology of phosphor shows a shape of octahedral crystals and the size is 1.5–2 μm. Under 466 nm excitation, the phosphor emits a series of narrow band emission lines centred at 630 nm. The PL properties of the $K_2NaGaF_6:Mn^{4+}$ red phosphors were optimized with different Mn^{4+} concentrations and aging times. Based on its excellent PL properties, a white-light-emitting diode was fabricated by a blue LED chip combined with commercial yellow YAG:Ce^{3+} phosphor and the synthesized $K_2NaGaF_6:Mn^{4+}$ red phosphor. The CCT and R_a value of this device reach 3643 K and 81.6 respectively. All these results imply that the $K_2NaGaF_6:Mn^{4+}$ red phosphor has potential applications in warm W-LEDs.

Conflicts of interest

There are no conflicts to declare.

Acknowledgements

The Project was sponsored by the National Natural Science Foundation of China (21401122, 51272151, and 51672167), the Natural Science Foundation of Shaanxi Province (2014JZ002, 2015JQ2041), Fundamental Research Funds for the Central Universities (GK201603050, GK201703020, and GK201701011), and Science and Technology program of Xi'an (2017071CG/RC034(SXSF004)).

References

1 A. Lazarowska, S. Mahlik, M. Grinberg, C. C. Lin and R. S. Liu, *J. Chem. Phys.*, 2015, **143**, 134704.
2 Y. Jin, M. H. Fang, M. Grinberg, S. Mahlik, T. Lesniewski, M. G. Brik, G. Y. Luo, J. G. Lin and R. S. Liu, *ACS Appl. Mater. Interfaces*, 2016, **8**, 11194–11203.
3 H.-D. Nguyen, C. C. Lin, M.-H. Fang and R.-S. Liu, *J. Mater. Chem. C*, 2014, **2**, 10268–10272.
4 L. Lv, X. Jiang, S. Huang, X. a. Chen and Y. Pan, *J. Mater. Chem. C*, 2014, **2**, 3879–3884.
5 R. Kasa and S. Adachi, *J. Electrochem. Soc.*, 2012, **159**, J89.
6 C. C. Lin, A. Meijerink and R. S. Liu, *J. Phys. Chem. Lett.*, 2016, **7**, 495–503.
7 L. Huang, Y. Zhu, X. Zhang, R. Zou, F. Pan, J. Wang and M. Wu, *Chem. Mater.*, 2016, **28**, 1495–1502.
8 Q. Zhou, Y. Zhou, Y. Liu, Z. Wang, G. Chen, J. Peng, J. Yan and M. Wu, *J. Mater. Chem. C*, 2015, **3**, 9615–9619.
9 W.-L. Wu, M.-H. Fang, W. Zhou, T. Lesniewski, S. Mahlik, M. Grinberg, M. G. Brik, H.-S. Sheu, B.-M. Cheng, J. Wang and R.-S. Liu, *Chem. Mater.*, 2017, **29**, 935–939.
10 L.-L. Wei, C. C. Lin, M.-H. Fang, M. G. Brik, S.-F. Hu, H. Jiao and R.-S. Liu, *J. Mater. Chem. C*, 2015, **3**, 1655–1660.
11 L. Y. Wang, E. H. Song, Y. Y. Zhou, T. T. Deng, S. Ye and Q. Y. Zhang, *J. Mater. Chem. C*, 2017, **5**, 7253–7261.
12 F. Tang, Z. Su, H. Ye, M. Wang, X. Lan, D. L. Phillips, Y. Cao and S. Xu, *J. Mater. Chem. C*, 2016, **4**, 9561–9568.
13 H. F. Sijbom, J. J. Joos, L. I. D. J. Martin, K. Van den Eeckhout, D. Poelman and P. F. Smet, *ECS J. Solid State Sci. Technol.*, 2015, **5**, R3040–R3048.
14 X. Li, X. Su, P. Liu, J. Liu, Z. Yao, J. Chen, H. Yao, X. Yu and M. Zhan, *CrystEngComm*, 2015, **17**, 930–936.
15 Y. Arai and S. Adachi, *J. Electrochem. Soc.*, 2011, **158**, 179.
16 Q. Zhou, Y. Zhou, Y. Liu, L. Luo, Z. Wang, J. Peng, J. Yan and M. Wu, *J. Mater. Chem. C*, 2015, **3**, 3055–3059.
17 J. S. Zhong, D. Q. Chen, X. Wang, L. F. Chen, H. Yu, Z. G. Ji and W. D. Xiang, *J. Alloys Compd.*, 2016, **662**, 232–239.
18 E. H. Song, J. Q. Wang, S. Ye, X. F. Jiang, M. Y. Peng and Q. Y. Zhang, *J. Mater. Chem. C*, 2016, **4**, 2480–2487.
19 E. Song, J. Wang, J. Shi, T. Deng, S. Ye, M. Peng, J. Wang, L. Wondraczek and Q. Zhang, *ACS Appl. Mater. Interfaces*, 2017, **9**, 8805–8812.
20 P. Rawat, S. Kumar Saroj, M. Gupta, G. Vijaya Prakash and R. Nagarajan, *J. Fluorine Chem.*, 2017, **200**, 1–7.
21 T. T. Deng, E. H. Song, J. Sun, L. Y. Wang, Y. Deng, S. Ye, J. Wang and Q. Y. Zhang, *J. Mater. Chem. C*, 2017, **5**, 2910–2918.
22 T. Deng, E. H. Song, Y. Y. Zhou, L. Y. Wang, S. Ye and Q. Zhang, *J. Mater. Chem. C*, 2017, **5**, 9588–9596.
23 Y. Zhu, J. Yu, Y. Liu, M. G. Brik, L. Huang, T. Xuan and J. Wang, *RSC Adv.*, 2017, **7**, 30588–30593.
24 Y. Zhu, L. Cao, M. G. Brik, X. Zhang, L. Huang, T. Xuan and J. Wang, *J. Mater. Chem. C*, 2017, **5**, 6420–6426.

25 L. Y. Wang, E. H. Song, T. T. Deng, Y. Y. Zhou, Z. F. Liao, W. R. Zhao, B. Zhou and Q. Y. Zhang, *Dalton Trans.*, 2017, **46**, 9925–9933.
26 D. Li, W. Qin, P. Zhang, S. Xiao and L. Wang, *CrystEngComm*, 2016, **18**, 6908–6913.
27 M. C. M. De Lucas, J. M. Dance, F. Rodríguez, A. Tressaud, M. Moreno and J. Grannec, *Radiat. Eff. Defects Solids*, 2006, **135**, 19–22.
28 M. G. Brik and K. Ogasawara, *Phys. Rev. B: Condens. Matter Mater. Phys.*, 2006, **74**, 045105.
29 Y. Zhu, Y. Liu, L. Huang, T. Xuan and J. Wang, *Sci. China: Technol. Sci.*, 2017, 6420–6426.
30 M. D. Segall, P. J. D. Lindan, M. J. Probert, C. J. Pickard, P. J. Hasnip, S. J. Clark and M. C. Payne, *J. Phys.: Condens. Matter*, 2002, **14**, 2717–2744.
31 M. J. Lee, Y. H. Song, Y. L. Song, G. S. Han, H. S. Jung and D. H. Yoon, *Mater. Lett.*, 2015, **141**, 27–30.
32 Z. Yang, Q. Wei, M. Rong, Z. Yang, Z. Wang, Q. Zhou and Q. Wang, *Dalton Trans.*, 2017, **46**, 9451–9456.
33 L. F. Lv, X. Y. Jiang, S. M. Huang, X. Chen and Y. X. Pan, *J. Mater. Chem. C*, 2014, **2**, 3879–3884.
34 Q. Zhou, H. Y. Tan, Y. Y. Zhou, Q. H. Zhang, Z. L. Wang, J. Yan and M. M. Wu, *J. Mater. Chem. C*, 2016, **4**, 7443–7448.
35 K. Inaba, S. Suzuki, Y. Noguchi, M. Miyayama, K. Toda and M. Sato, *Eur. J. Inorg. Chem.*, 2008, **35**, 5471–5475.
36 J. Zhuang, X. Zhang, G. Wang, D. Li, W. Yang and T. Li, *J. Mater. Chem.*, 2003, **13**, 1853–1857.
37 X. Zhang, J. Yu, J. Wang, B. Lei, Y. Liu, Y. Cho, R.-J. Xie, H.-W. Zhang, Y. Li, Z. Tian, Y. Li and Q. Su, *ACS Photonics*, 2017, **4**, 986–995.
38 A. Wang, X. Yan, M. Zhang, S. Sun, M. Yang, W. Shen, X. Pan, P. Wang and Z. Deng, *Chem. Mater.*, 2016, **28**, 8132–8140.
39 Z. Liang, S. Zhao, Z. Xu, B. Qiao, P. Song, D. Gao and X. Xu, *ACS Appl. Mater. Interfaces*, 2016, **8**, 28824–28830.